Spherically symmetric models for x-ray damage and the movement of electrons produced in non-spherically symmetric targets such as bio-molecules

J. Phys. B: At. Mol. Opt. Phys. **43** (2010) 165602 (7pp) doi:10.1088/0953-4075/43/16/165602

Spherically symmetric models for x-ray damage and the movement of electrons produced in non-spherically symmetric targets such as bio-molecules

Kengo Moribayashi

Japan Atomic Energy Agency, 8-1, Umemidai, Kizugawa-city 619-0215, Japan

E-mail: moribayashi.kengo@jaea.go.jp

Received 25 March 2010, in final form 22 June 2010
Published 30 July 2010
Online at stacks.iop.org/JPhysB/43/165602

Abstract
This paper develops spherically symmetric models as well as a more accurate model for the calculation of the damage and the movement of free and quasi-free electrons which are produced from the irradiation of x-ray free electron lasers (XFELs). The behaviour of free and quasi-free electrons is studied for targets with various shapes such as spheres and ellipsoids by treating the space distribution of free and quasi-free electrons. Furthermore, the limits of the application of spherically symmetric models to various shapes are discussed. The spherically symmetric model developed here is also applied to a bio-molecule. The results obtained are useful for the analysis of the three-dimensional structures of large bio-molecules in the experiments of XFELs.

1. Introduction

The study of the damage and destruction of bio-molecules due to the irradiation of x-ray free electron lasers (XFELs) is indispensable for the analysis of three-dimensional (3D) structures using non-crystallized single bio-molecules [1–13]. We define the damage and the destruction as the ionization and the movement of atoms in a target, respectively [6, 7]. This comes from the fact that the positions of the atoms do and do not change due to the movement and the ionization, respectively. The change of the positions means that the reconstruction of the 3D structure cannot be executed. The damage and the destruction mainly occur through the following occurrences. (i) The atoms in the target are ionized through x-ray absorption or Compton scattering. (ii) From these ionization processes, free electrons, quasi-free electrons and ions are produced and move, where we define 'a free electron' and 'a quasi-free electron' as an electron, which is ionized from an atom, outside and inside the target, respectively [4]. (iii) Quasi-free electrons promote the ionization of other atoms through electron impact ionization processes. (iv) Other ionization processes, such as Auger, also occur.

The analysis of 3D structures of bio-molecules is executed based on diffraction patterns which come from x-rays scattered by electrons bounded in atoms. The intensity of the diffraction patterns (I_o) is given by

$$I_o(\vec{k}) \propto I_i |F(\vec{k})|^2, \tag{1}$$

where I_i is the intensity of an XFEL, and $F(\vec{k})$ defined by

$$F(\vec{k}) = \int \rho(\vec{r})\, \mathrm{e}^{\mathrm{i}\vec{k}\bullet\vec{r}}\, \mathrm{d}\vec{r} = \sum_i \mathrm{e}^{\mathrm{i}\vec{k}\bullet\vec{r}_i} \int \rho_{\mathrm{atom}}(\vec{r})\, \mathrm{e}^{\mathrm{i}\vec{k}\bullet\vec{r}}\, \mathrm{d}\vec{r} + \int \rho_{\mathrm{fe}}(\vec{r})\, \mathrm{e}^{\mathrm{i}\vec{k}\bullet\vec{r}}\, \mathrm{d}\vec{r} \tag{2}$$

is the structure factor as a function of wave number vectors ($\vec{k}$) with $\vec{k} = \vec{K}_i - \vec{K}_f$. Here $\vec{r}_i$, $\rho(\vec{r})$, $\rho_{\mathrm{atom}}(\vec{r})$ and $\rho_{\mathrm{fe}}(\vec{r})$ are the position of an atom in the target, the electron density in the bio-molecule, the electron density in the atom and the density of free and quasi-free electrons, respectively, and $\vec{K}_i$ and $\vec{K}_f$ are the wave number vectors of the incident and scattered x-rays, respectively. It should be noted that the second term on the right-hand side of equation (2) is conventionally ignored because $\rho_{\mathrm{fe}}(\vec{r})$ is too small. As seen in equation (1), in diffraction patterns, the information on the phases of $F(\vec{k})$ has disappeared. In order to get three-dimensional

structures, the phase recovery for the first term on the right-hand side of equation (2) is required using the repetition of Fourier transfer simulations such as an over-sampling method [11, 12]. Further, the change of $\rho_{\rm atom}(\vec{r})$ and the positions of atoms during the irradiation of x-rays are also conventionally ignored because of the small amount of damage and destruction. On the other hand, in XFEL light pulses, we may need to consider this second term on the right-hand side of equation (2), the change of $\rho_{\rm atom}(\vec{r})$ and the positions of atoms because of the larger damage. Namely, the damage and the destruction change the diffraction patterns due to (i) ionization processes, which reduce I_o; then we should change $\rho_{\rm atom}(\vec{r})$ to the electron density according to the ionized states [$\rho_{\rm ion}(\vec{r})$] using the method given in [13]; (ii) the interference of x-rays scattered by electrons bounded in the atoms with those by quasi-free and free electrons, which changes I_o (see the second term on the right-hand side of equation (2)); (iii) the movement of atoms, which changes $\vec{r}_i$. For the movement of atoms, the distances over which the atoms move become one of the factors in the decision of the highest resolving power of the 3D structures obtained from the experiments. Therefore, we need to control these distances to be smaller than the desired resolving power during the irradiation of XFEL light pulses on the target. However, the movement of atoms may be able to be controlled using a short pulse of XFELs [1] or a tamper target [5], where the latter is defined as a bio-molecule surrounded by multi-layers of water. Hau-Riege *et al* [5] showed from their simulation that the movement of atoms can be controlled using a tamper target and a pulse of 50 fs as diffraction patterns change little. On the other hand, it is almost impossible to control the movement of electrons. This means that the effect of the movement of atoms on the analysis of 3D structures is much smaller than that of the movement of electrons. Here we include the movement of electrons and exclude the movement of atoms in our simulations, although we do not think that the movement of atoms can be ignored. We will address this in the future.

Before we commence the experiments of diffraction patterns, simulations of the damage and the destruction play an important role. The simulations have been executed using various methods, such as molecular dynamics (MD) [1–3], rate equations [4–7, 9, 10] and kinetic Boltzmann equations [8]. All of these methods have advantages and disadvantages. In MD, accurate simulation can be executed for bio-molecules of small size, having up to 10 000 atoms. However, MD is unsuitable for larger sizes because it takes too much time to calculate the damage and the movement of electrons and ions. The rate equations and the kinetic Boltzmann equations can treat bio-molecules of larger size using spherically symmetry models, that is, one-dimensional models. If spherically symmetrical models are applicable, then the interaction between individual charged particles does not have to be calculated, which saves computing time. However, there are no papers that discuss the limits of the application of spherical symmetrical models to the shape of the targets as far as we know. Therefore, in this paper, we confirm these limits. Further, we develop a spherically symmetrical model based on the Gauss law for spheres, which is able to treat the movement of free and quasi-free electrons (see section 2.4). We compare the movement of free and quasi-free electrons calculated by our spherically symmetric model with those of a more accurate one, that is, the Monte Carlo and Newton equation (MCN) model (see section 2.3 and [9]) for various target shapes in order to study the accuracy of our spherically symmetric model. We hope that our model and the information from its application will help in simulating larger sizes of bio-molecules using the rate equations or kinetic Boltzmann equations.

2. Method of calculations

2.1. Setups of the positions of atoms and parameters of XFEL light pulses

First, we treat model carbon clusters with various shapes such as spheres and ellipsoids at a solid density (3×10^{22} cm^{-3}) in order to develop simulation models. We choose positions inside and outside the target from the number and the density of atoms. Then the positions of the atoms are assigned randomly on the condition that they are located inside the target and that lengths among the atoms are larger than 3 Å, which is almost the same as the length between carbons in proteins. Then we attempt to apply our models to one bio-molecule, that is, a lysozyme which has the elements H, N, O and S, as well as C. We use the coordinate data of a lysozyme in the protein data bank (PDB) (http://www.pdb.org/pdb/home/home.do), in which we employ 2LZM as PDB ID.

For the parameters of XFEL light pulses, it is estimated that x-ray fluxes around 10^{20} photons/pulse/mm^2 and wavelength around 1 Å are required [1, 4, 6]. In this paper, we treat x-ray fluxes of 10^{20} to 5×10^{20} photons/pulse/mm^2, a wavelength of 1 Å, a pulse of 10 fs and the number of atoms of 1000–8000.

2.2. Ionization processes

Ionization processes treated here are x-ray absorption (e.g. C + $h\nu \rightarrow$ C$^+$ + e$^-$), Compton scattering (e.g. C + $h\nu \rightarrow$ C$^+$ + e$^-$ + $h\nu'$), electron impact ionization (e.g. C + e$^-$ $\rightarrow$ C$^+$ + 2e$^-$) and Auger (e.g. C^{+*} $\rightarrow$ C^{2+} + e$^-$), where $h\nu$ and $h\nu'$ are the x-ray energies before and after the process occurs, respectively. We calculate the change of both the ionized and excited states of the atoms and the production of free and quasi-free electrons using rates or cross sections of these ionization processes as a function of time. We use the same rates or cross sections as given in [7, 10, 14, 15]. The x-ray absorption cross sections ($\sigma_{\rm xa}$) are roughly calculated by

$$\sigma_{\rm xa} \propto |\langle f|\vec{r}|i\rangle|^2, \tag{3}$$

where $|i\rangle$ and $|f\rangle$ are the wavefunctions for the initial and final states, respectively [16]. On the other hand, the cross sections of Compton scattering ($\sigma_{\rm CS}$) are determined by the Klein–Nishina formula [17, 18], that is,

$$\frac{{\rm d}\sigma_{\rm CS}}{{\rm d}\Omega} = \frac{1}{2} r_c^2 \frac{(h\nu')^2}{(h\nu)^2} \left(\frac{h\nu}{h\nu'} + \frac{h\nu'}{h\nu} - \sin^2\theta \right), \tag{4}$$

where r_c, θ and Ω are the radius of a classical electron, the scattering angle and the solid angle, respectively, and $h\nu'$ is given by

$$h\nu' = \frac{h\nu}{1 + \frac{h\nu}{m_e c^2}(1 - \cos\theta)}, \tag{5}$$

where m_e and c are the mass of an electron and the speed of light, respectively. Then the rates of the x-ray absorption ($R_{\rm xa}$) and Compton scattering ($R_{\rm CS}$) are given by

$$R_{\rm xa} = \frac{I\sigma_{\rm xa}}{h\nu} \qquad \text{and} \qquad R_{\rm CS} = \frac{I\sigma_{\rm CS}}{h\nu}, \tag{6}$$

respectively, where I is the intensity of the x-rays [19, 20]. On the other hand, Auger rates are roughly given by

$$A_a \propto \left| \langle f | \frac{1}{r_{12}} | \mathrm{i} \rangle \right|^2, \tag{7}$$

where r_{12} is the length between an electron transferred from an excited state to the ground state and that ionized from an ion [7, 16]. We have used the Auger rates given in [7]. For the cross sections of the electron impact ionization processes (σ_e), we employ the data listed in [14].

The initial energies and velocities of electrons produced from these ionization processes should be mentioned because they contribute significantly not only to the movement of free and quasi-free electrons but also to the treatment of electron impact ionization processes. (i) X-ray absorption processes: the initial electron energy corresponds to the value that subtracted a bound energy (E_B) of atoms or ions from the x-ray energy. Since the x-ray energy treated here is much larger than E_B of H, C, N and O, which are the main elements of bio-molecules, the initial electron energy is almost the same as the x-ray energy. (ii) Compton scattering: the value of θ is determined randomly by treating the right-hand side of equation (4) multiplied by dΩ as a weighting factor and the initial electron energy is $h\nu - h\nu' - E_B$. (iii) Auger: we employ the initial electron energy calculated by Cowan's code [16]. (iv) Electron impact ionization processes: we calculate the initial electron energy from binary encounter dipole (BED) theory [10, 21] or use the data given in [22]. After the initial electron energy is determined, the initial direction of the electron velocity is given randomly except for that due to Compton scattering. In Compton scattering, the initial direction is determined from the electron energy, θ, and the momentum conservation law.

2.3. Monte Carlo and Newton equation model

The MCN model employed here is almost the same method as that treated in [2, 3] except for the movement of atoms or ions as mentioned in section 1. The x-ray absorption, Auger and Compton scattering processes are treated using the Monte Carlo method as follows [23] (i) When an XFEL light pulse begins to irradiate a target, we start the calculation and set the time $t = 0$. We also set the neutral and the ground states for ionized and excited states of all atoms in the target, respectively. (ii) We calculate the transition rates [$R_{ifp}(m)$] (see section 2.2) of all the possible ionization processes according to the ionized and excited states of all the atoms and random numbers [$N_R(m)$]. One random number is given to each atom at the time interval between t and $t + \Delta t$, where $R_{ifp}(m)$ and N_R (m) are the transition rate from the ith state to the fth one of the mth atom due to the pth ionization process and the random number given to the mth atom, respectively. We take Δt to be 2×10^{-3} fs. (iii) Only when

$$\sum_p \sum_f R_{ifp}(m)\Delta t > N_R(m), \tag{8}$$

one process for the mth atom occurs. When equation (8) is satisfied, the state where the ionization occurs is chosen randomly among all the possible transitions using the respective $R_{ifp}(m)$ as weighting factors. (iv) The value of t increases by Δt and procedures (ii) and (iii) are executed. (v) We reiterate procedures (ii)–(iv) until the XFEL light pulse passes through the target.

For the electron impact ionization process, a similar method to that treated in [2, 3] is employed. It is judged that the process occurs only when a quasi-free electron crosses the area of a cross section according to an ionized state of an atom. The centre of the cross section is located at the atomic nucleus and the cross section is perpendicular to the direction of the electron velocity.

The Coulomb forces due to ions and electrons act on free and quasi-free electrons. The movement of these electrons is solved by the Newton equations, that is,

$$\vec{F} = m_e \frac{\mathrm{d}\vec{v}_{\rm ei}}{\mathrm{d}t} = -\sum_{j \neq i} \frac{e^2 \vec{r}_{ij}}{4\pi\varepsilon_0 r_{ij}^3} + \sum_l \frac{q_l e \vec{r}_{il}}{4\pi\varepsilon_0 r_{il}^3}, \tag{9}$$

where ε_0, m_e, $\vec{v}_{ei}$, q_l and $\vec{r}_{ij(l)}$ are the dielectric constant in vacuum, the mass of an electron, the velocity of the ith electron, the charge of the lth ion and the distances between the ith electron and the jth free and quasi-free electron (the lth ion), respectively [9]. In order to avoid divergence near $r_{ij(l)} = 0$ in equation (9), we use a similar approximation to that employed in [2, 3], that is, $r_{ij(l)}$ is approximately replaced by $\left(r_{ij(l)}^2 + a_s^2\right)^{1/2}$, where we take a_s to be 1 Å. We use Δt given in equation (8) as a time step for the movement of the electrons.

It should be noted that the production and the movement of electrons depend on the initial values of the random numbers (seeds) and that we can demonstrate the calculations of the damage and the electron distributions for different pulses using different initial seeds for the random number generated. We show the results averaged by a few hundred pulses in section 3.

2.4. Spherically symmetric models

In the case of a spherical target with a radius of 100 nm, the number of atoms is larger than 10^7. In our calculation using the MCN developed here, it takes about 12 h to calculate the damage and the movement of free and quasi-free electrons for the number of atoms of only 8000 and the x-ray flux of 3×10^{20} photons/pulse/mm^2. Therefore, it takes too much time to execute the 3D calculation for the damage of bio-molecules

when we treat a target with a radius around 100 nm. Then spherically symmetric models become useful.

When we study the irradiation of XFEL light pulses with the clusters or bio-molecules, the uniform space charge $Q_e(r)$ is produced from electrons escaping from the target [9], that is,

$$\begin{aligned} Q_e(r) &= \tfrac{4}{3}\pi r^3 D_{ee} e \qquad (r < r_0) \\ Q_e(r) &= \tfrac{4}{3}\pi r_0^3 D_{ee} e \qquad (r \geqslant r_0), \end{aligned} \tag{10}$$

with $D_{ee} = N_{ee}/V_t$, where r_0, e, N_{ee} and V_t are the radius of the target, the charge of an electron, the number of the electrons which escape from the target and the volume of the target, respectively [9]. This comes from the Gauss law for the sphere [9]. Then, in our first approximation (which we call the SSM1), we use equation (10) for the space charge, where the uniform charge distribution in the spherical targets is assumed. In the case of ellipsoids, we define an escaped electron as an electron which has a value of r larger than that of the atom furthest from the centre of the target (r_{alm}), that is, $r_0 = r_{alm}$. From equation (10), the force acting on an electron becomes

$$\begin{aligned} F(r) &= \frac{Q_e(r)e}{4\pi\varepsilon_0 r^2} = \frac{1}{3\varepsilon_0} r D_{ee} e^2 \qquad (r < r_0) \\ F(r) &= \frac{Q_e(r_0)e}{4\pi\varepsilon_0 r^2} \qquad (r \geqslant r_0). \end{aligned} \tag{11}$$

Here, the force is directed towards the centre. It should be noted that equation (11) follows the Gauss law in the case of uniform charge distribution in spherical targets. Namely the electric fields ($F(r)/e$) are produced from the charge, which exists inside the location of interest, and the charge outside it can be ignored because of cancellation. We treat equation (11) instead of equation (9) for the movement of electrons in the SSM1. In equation (11), there is no divergence near $r = 0$, which often appears for the point charge because $F(0) = 0$. This approximation is usable only when the number of quasi-free electrons is too small to affect the charge distribution. Since the SSM1 is useful for saving the calculation time, we examine the limits of application of the SSM1. When we consider that quasi-free electrons affect the charge distribution, the charge distribution for r becomes non-uniform. Then in our second approximation (SSM2), we estimate the charge $Q_{es}(r)$ by counting the total charge inside the location where the electron of interest exists and we use $Q_{es}(r)$ instead of $Q_e(r)$ in equation (11).

3. Results and discussion

Here the behaviour of free and quasi-free electrons is discussed from the space electron distribution. We treat the x-ray fluxes of 10^{20}, 3×10^{20} and 5×10^{20} photons/pulse/mm^2 and the number of atoms of 1000, 2000, 4000 and 8000. We have found almost the same trends for the electron distribution for all the parameters. Here we show only the case of the x-ray flux of 3×10^{20} photons/pulse/mm^2 and the number of atoms of 2000.

Figure 1 shows the free and quasi-free electron distribution as a function of r for a spherical target at $t =$ 1 attosecond (as), 1, 3 and 9 femtosecond (fs) calculated by the MCN, the SSM1 and the SSM2, where r is the distance from the centre of the target. We set the time of $t = 0$ just when an XFEL light pulse begins to irradiate the target. The electron distribution treated here is defined as follows. (i) We count the number of electrons [$N_e(r)$] at the interval between r and $r + \Delta r$, where we take Δr to be 1 Å. (ii) The electron distribution F_{ed} (r) is given by

$$F_{ed}(r) = \frac{N_e(r)}{4\pi\left(r + \frac{\Delta r}{2}\right)^2}. \tag{12}$$

The results calculated by the SSM1 and SSM2 show good agreement with those of the MCN at $t = 1$ as and 1 fs (see figures 1(a) and (b)). At 1 as (see figure 1(a)), the distribution becomes almost a constant value as a function of r except for those near the surface. The behaviour near the surface comes from the fact that quasi-free electrons produced near the surface can escape from the target even at 1 as. At 1 fs (see figure 1(b)), many quasi-free electrons can escape from the target. Then the distribution becomes smaller as r increases. We predict from figure 1(b) as follows. (i) Since quasi-free electrons are accelerated towards $r = 0$, the electrons become concentrated near $r = 0$. (ii) As the charge becomes smaller near $r = 0$, the acceleration becomes weaker as time progresses. (iii) This reduces the invasion of quasi-free electrons into $r = 0$. As a result, the distribution near $r = 0$ becomes almost a constant value as a function of r (see figures 1(c) and (d)). This trend agrees well with that given by [4]. For $t \geqslant 3$ fs (see figures 1(c) and (d)), the SSM1 seems to become useless because the number of quasi-free electrons is large enough to affect the charge distribution. The electron distribution calculated by the SSM2 still shows good agreement with that of the MCN except for points near $r = 0$.

In order to verify the behaviour of the electron distribution shown in figure 1 in more detail, we have calculated electric fields. Figure 2 shows the electric fields on the x-axis as a function of x for the spherical target at $t = 1$, 3 and 9 fs. Here we take randomly one direction from the centre as the x-axis because we treat spherical targets where spherical symmetry, that is, the one-dimensional model, can be adopted. In figure 2, the MCN and the SSM2 are employed. We have found from the results calculated by the MCN in figure 2(a) that the electric fields show similar trends to those obtained from the Gauss law in the case of the uniform space charge distribution in spherical targets. Namely, the electric fields increase almost in proportion to x until they reach the surface of the target and then decrease beyond the surface. The y- and z-components of the electric fields are much smaller than their x-component. On the other hand, for $t \geqslant 3$ fs (see figures 2(b) and (c)), the electric fields become much smaller except for those near the surface of the target. This comes from the invasion of quasi-free electrons into $r = 0$ and then causes the SSM1 to become useless because the charge distribution becomes non-uniform for r. Further, we have found that the y- and z-components of the electric fields become comparable to their x-component near $x = 0$ in the MCN. This may come from the facts that the number of charged particles inside the location of interest is much

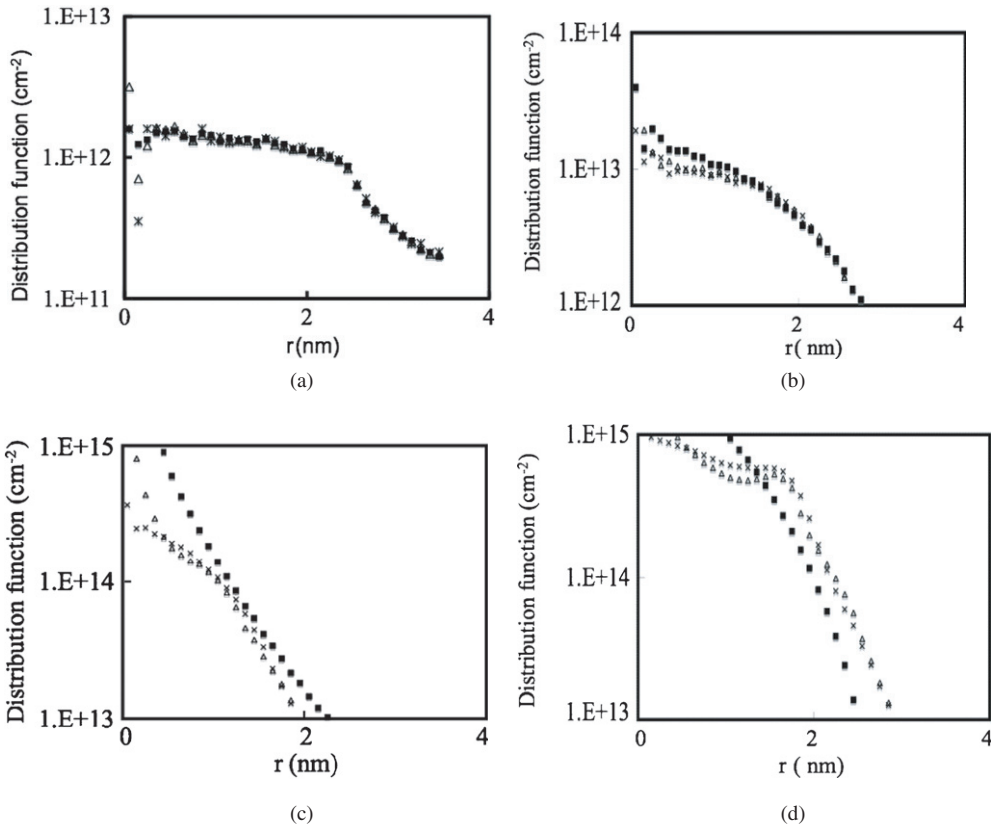

Figure 1. Electron distribution defined by equation (12) versus r at (a) $t = 1$ as, (b) $t = 1$ fs, (c) $t = 3$ fs and (d) $t = 9$ fs for a spherical target. The calculation methods are the MCN (×), the SSM1 (■) and the SSM2 (△). The x-ray fluxes, the number of atoms in a target, the wavelength and the pulse of XFEL are 3×10^{20} photons/pulse/mm^2, 2000, 1 Å and 10 fs, respectively.

smaller than that outside it and the charge distribution outside the location of interest is not perfectly symmetrical. In the case of perfect symmetry, the cancellation occurs for electric field contributions from charged particles outside the location of interest as mentioned before. However, the cancellation near $x = 0$ may become insufficient in figures 2(b) and (c) because of the large number of quasi-electrons outside the locations of interest and non-perfect symmetry. As a result, we may not be able to ignore the charge distribution outside it near $x = 0$ in the MCN. On the other hand, in the SSM2, only the charge inside it is considered (see section 2.4). This gives rise to a disagreement between the electron distributions near $r = 0$ given by the MCN and the SSM2 (see figures 1(c) and (d)).

From here, we do not treat the SSM1 because we have judged from figure 1 that it is dangerous to apply the SSM1 to the calculation of the electron distribution. Figure 3 shows the same as figure 1(d) ($t = 9$ fs) for $l_r = 2$, 3 and 4, where l_r is the ratio of the lengths of the major axis with that of the minor one in the ellipsoid. We have found the same tendency as that in figure 1(d) at $l_r = 2$ and 3 (see figures 3(a) and (b)), that is, the electron distribution near $r = 0$ remains almost a constant value, and good agreement between the electron distributions calculated by the SSM2 and the MCN is shown. As l_r increases, the discrepancy between the electron distributions calculated by the SSM2 and the MCN becomes larger. At $l_r = 4$, the flat appearance near $r = 0$ seems to disappear. Since there is a big difference in the electron distribution calculated by the MCN with that by the SSM2 at $l_r = 4$, our spherically symmetric models may no longer be applied for $l_r = 4$.

Figure 4 shows the same as figures 1(d) and 3 ($t = 9$ fs) for the application to a lysozyme. A lysozyme has the elements H, N, O and S, as well as C. We treat the ionization processes using cross sections or rates corresponding to each element except for S because the proportion of S is much smaller than that of the other elements. We have found the same trends as those in figure 1(d), that is, the electron distribution near $r = 0$ remains almost a constant value and good agreement between the electron distributions calculated by the SSM2 and the MCN is shown. This may result from the fact that a lysozyme has a shape close to a sphere as follows. We derive the relationship between the radius of the sphere into which the bio-molecule could be transformed (r_{0t}) and the average value among the lengths of the places of atoms from the centre (r_{av}). The relationship between r_{av} and r_{0t} is given by

$$r_{\mathrm{av}} = \frac{\int_0^{r_{0t}} r 4\pi r^2 \,\mathrm{d}r}{\frac{4}{3}\pi r^3} = \frac{3}{4} r_{0t}, \tag{13}$$

that is, we assume $r_{0t} = 4/3\ r_{\mathrm{av}}$. From this equation, we estimate that r_{0t} and l_r for a lysozyme are approximately 21 Å

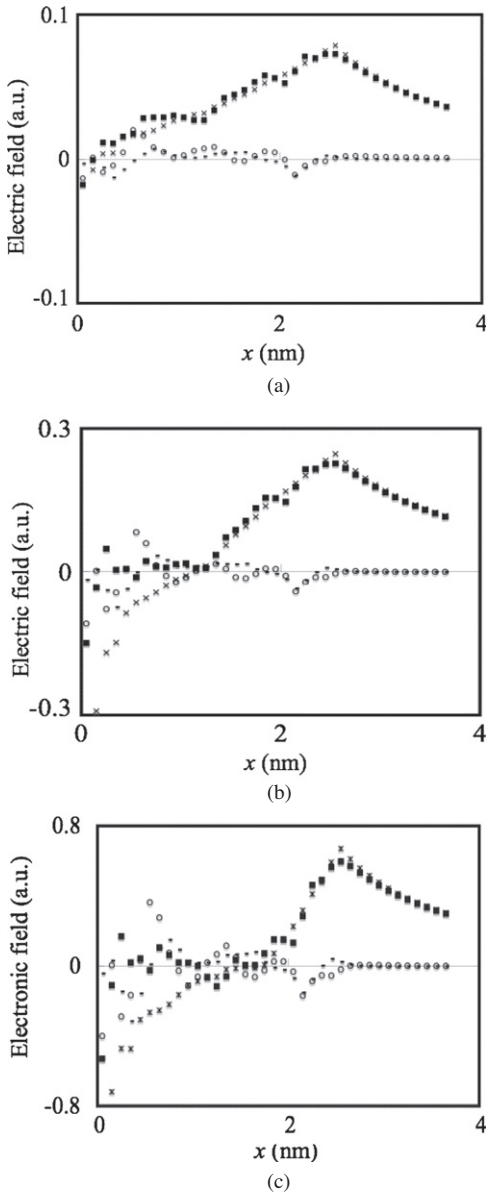

Figure 2. Electric field on the x-axis versus x model at (a) $t = 1$ fs, (b) $t = 3$ fs and (c) $t = 9$ fs for a spherical target. The calculation methods are the SSM2 (×) and the MCN. In the MCN, the x-component (■), y-component (–) and z-component (□) of the electric fields are shown. The x-ray fluxes, the number of atoms in a target, the wavelength and the pulse of XFEL are 3×10^{20} photons/pulse/mm^2, 2000, 1 Å and 10 fs, respectively.

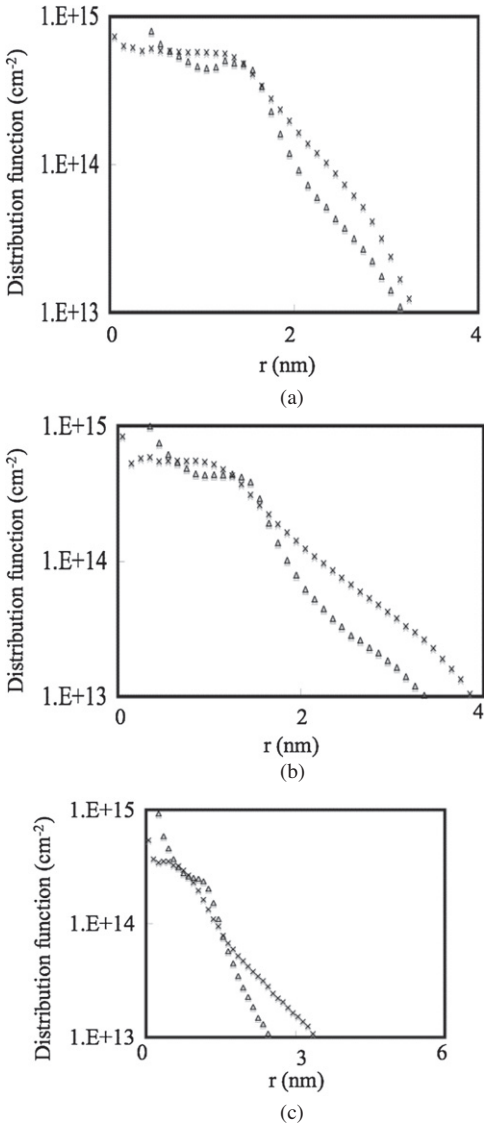

Figure 3. The same as figure 1(d) for (a) $l_r = 2$, (b) $l_r = 3$ and (c) $l_r = 4$. The calculation methods are the MCN (×) and the SSM2 (△).

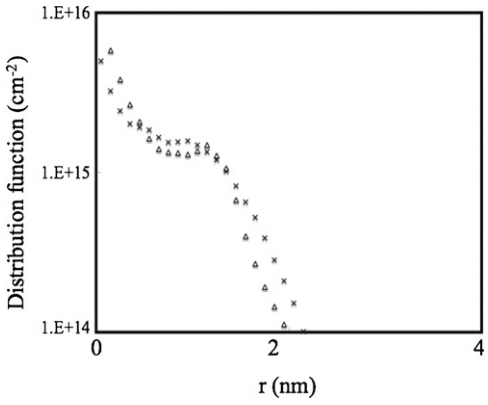

Figure 4. The same as figure 1(d) for the target of a lysozyme. The calculation methods are the MCN (×) and the SSM2 (△).

and about 1.35, respectively. We conclude that we may apply the SSM2 to the calculation of the electron distribution on bio-molecules with shape close to a sphere.

The 3D structures of bio-molecules which cannot be crystallized will be constructed from diffraction patterns, which are produced from x-rays scattered by the bound electrons in atoms in the target. On the other hand, x-rays scattered by quasi-free electrons obtained here interfere with those by the bound electrons in the atoms and the interference appears as a noise for the diffraction patterns observed on the x-ray detectors. For the calculation of this noise, we hope that our spherically symmetrical model becomes useful for large bio-molecules.

4. Summary

We have developed spherically symmetric models and a more accurate model applied to the calculation of the damage of bio-molecules and the movement of free and quasi-free electrons for targets with various shapes such as spheres and ellipsoids. The damage and the free and quasi-free electrons are produced from the irradiation of XFELs on the target. We discuss the space distribution of free and quasi-free electrons. The electron distribution calculated by our spherically symmetric model agrees well with that calculated by our more accurate model except for the point near the centre of the targets with $l_r = 1$–3, where l_r is the ratio of the lengths of the major axis with that of the minor one in the ellipsoid. However, we have found a big difference between the electron distributions calculated by the MCN and SSM2 models at $l_r = 4$ and our spherically symmetric model may no longer be applied for $l_r \geqslant 4$. Our spherically symmetric model can be applied to a lysozyme. We may apply our spherically symmetric models developed here to the calculation of the movement of free and quasi-free electrons in bio-molecules with a shape close to a sphere.

Acknowledgments

We wish to thank Professor N Go, Doctors H Kono, T Kai, A Tokushisa, J Koga and M Yamagiwa for their useful discussions. This study has been supported by the 'X-ray Free Electron Laser Utilization Research Project' of the Ministry of Education, Culture, Sports, Science and Technology of Japan (MEXT). We employ the data in the protein data bank (PDB) for the position coordinate of a lysozyme.

References

[1] Neutze R, Wouts R, Spoel D, Weckert E and Hajdu J 2000 *Nature* **406** 752
[2] Jurek Z, Faigel G and Tegze M 2004 *Eur. Phys. J.* D **29** 217
[3] Jurek Z and Faigel G 2008 *Eur. Phys. J.* D **50** 35
[4] Hau-Riege S P, London R A and Szoke A 2004 *Phys. Rev.* E **69** 051906
[5] Hau-Riege S P, London R A, Chapman H N, Szoke A and Timneanu N 2007 *Phys. Rev. Lett.* **98** 198302
[6] Moribayashi K and Kai T 2009 *J. Phys.: Conf. Ser.* **163** 012097
[7] Moribayashi K 2008 *J. Phys. B: At. Mol. Opt. Phys.* **41** 085602
[8] Ziaja B, de Castro A R B, Weckert E and Möller T 2006 *Eur. Phys. J.* D **40** 465
[9] Moribayashi K 2009 *Phys. Rev.* A **80** 025403
[10] Kai T and Moribayashi K 2009 *J. Phys.: Conf. Ser.* **163** 012035
[11] Song C, Johnson D R, Nishino Y, Kohmura Y, Ishikawa T, Chen C C, Lee T K and Miao J 2007 *Phys. Rev.* B **75** 012102
[12] Gaffney K J and Chapman H N 2007 *Science* **316** 1444
[13] Hau-Riege S P 2007 *Phys. Rev.* A **76** 042511
[14] Bell K L, Gilbody H B, Hughes J G, Kingston A E and Smith F J 1983 *J. Phys. Chem. Ref. Data* **12** 891
[15] Henke B L, Gullikson E M and Davis J C 1993 *At. Data Nucl. Data Tables* **54** 181
[16] Cowan R D 1968 *J. Opt. Soc. Am.* **58** 808
[17] Klein V O and Nishina Y 1929 *Z. Phys.* **52** 853
[18] Blumenthal G R and Gould R J 1970 *Rev. Mod. Phys.* **42** 237
[19] Moribayashi K, Sasaki A and Tajima T 1998 *Phys. Rev.* A **58** 2007
[20] Moribayashi K 2007 *Phys. Rev.* A **76** 042705
[21] Kim Y K, Santos J P and Parente F 2000 *Phys. Rev.* A **62** 052710
[22] Nakazaki S, Nakashima M, Takebe H and Takayanagi K 1991 *J. Phys. Soc. Japan* **60** 1565
[23] Moribayashi K 2007 *J. Phys.: Conf. Ser.* **58** 192